Tuned Passive Control of Combustion Instabilities Using Multiple Helmholtz Resonators

Dan Zhao [a,*] A.S. Morgans [b]

[a] *Department of Engineering, University of Cambridge, Trumpington Street, Cambridge CB2 1PZ, UK*

[b] *Department of Aeronautics, Imperial College London, SW7 2AZ, London, UK*

Abstract

In this work, tuned passive control is used to damp unstable combustion systems, with particular emphasis on systems which exhibit multiple unstable modes. Helmholtz resonators are used as passive dampers. The frequency at which they offer maximum damping is varied by altering their geometry; in this work, geometry changes are achieved by varying the area of the Helmholtz resonator neck. For each unstable mode exhibited by the combustion system, a separate Helmholtz resonator has its neck area tuned. Two algorithms are developed, one for identifying the characteristics of all modes present in real-time, and another for tuning the neck areas of the Helmholtz resonators. These algorithms are successfully implemented in numerical simulations of a longitudinal combustor exhibiting two unstable modes. The algorithms result in both modes being stabilised as long as two Helmholtz resonators are used. Experiments are then conducted on a Rijke tube with its upper part split into two branches of differing lengths, shaped like a 'Y'. The differing lengths give rise to two unstable modes at different frequencies. A Helmholtz res-

onator is attached to each branch; the neck area of both can be varied by means of an 'iris' valve, which opens and closes like a camera lens. On implementing the procedure for tuning the neck areas, both unstable modes are stabilised, and stability is maintained for large changes in operating condition. This confirms that the procedure developed is sufficiently robust for use in real combustion systems exhibiting multiple unstable modes.

Key words: combustion instabilities, Helmholtz resonators, tuned passive control

1 Introduction

The drive for low NOx emissions means that gas turbine combustors (in both stationary power gas turbines and aero-engines) are being operated under lean premixed conditions. This makes them particularly susceptible to damaging combustion instabilities. Combustion instabilities are self-excited oscillations generated by the interaction between acoustic waves and combustion. Unsteady heat release generates acoustic waves; these propagate within the combustor and reflect from boundaries to arrive back at the combustion zone, where they cause more unsteady heat release. Under certain conditions, this feedback can result in large and damaging self-excited oscillations [1].

Typically, combustion instabilities are attenuated using either active or passive control by breaking the coupling between unsteady heat release and acoustic waves [2, 3]. Active control techniques involve a control system and use a dynamic actuator such as a loudspeaker or fuel supply valve. The actuator

* Corresponding author
Email address: DZ227@cam.ac.uk (Dan Zhao).

'perturbs' the state of the combustion system according to measurements to interrupt the coupling between the pressure and the heat release. If the way in which the actuator responds to the measurements has been designed correctly, the system will be stabilized. Active controllers are fast responding, as actuation occurs on the time scale of the instabilities. However, at industrial-scales, fuel modulation is the most viable form of actuation, and the bandwidth of the fuel valve becomes a limiting effect. Active control also has the potential to make the system more unstable.

Passive control techniques generally add acoustic damping to the combustion system. They are unlikely to make the system more unstable, but tend to be effective only over a narrow frequency range and are unable to respond to changes in operating conditions. Helmholtz resonators (HRs) have been widely used as acoustic dampers [4]. Their damping mechanism is primarily due to thermo-viscous and vortex shedding losses [5–7]. At resonance, a large volume of fluid in the chamber compresses and expands periodically, while a mass of the fluid in the neck vibrates. The resonant frequency of HRs is given approximately by $\omega^2 = c^2 S/V l_{\text{eff}}$ [8], where S and l_{eff} are the neck area and effective length of the neck respectively, V is the cavity volume and c is the ambient speed of sound. The fact that the resonant frequency depends on the geometry allows it to be tuned via geometry changes [9–15].

Tuned passive control involves using a control system to tune passive devices, such as Helmholtz resonators, in response to changes in the operating conditions. The feature of tunability overcomes the main disadvantage of traditional passive control. Moreover, actuation only needs to be on the time scale of the changes in operating condition, which is typically much slower than the time scale of the instability. The required actuator bandwidth is therefore small,

representing a major advantage over active control. Tuned passive control approaches therefore combine many of the advantages of active and passive control.

The resonant frequency of a Helmholtz resonator can be varied by adjusting the cavity volume, the neck area or the neck length. Several authors [9, 12, 14] have developed Helmholtz resonators with a variable cavity volume. A volume-variable resonator may be the easiest to implement in practice, but at low frequencies becomes unnecessary bulky [16]. In addition, serious sealing issues can arise. Helmholtz resonators with adjustable neck areas have also been considered, although not widely [11, 13].

In this paper, Helmholtz resonators are used for passive control. They are tuned to the measured modal frequencies by varying their neck areas. This avoids the sealing issues that occur when the volume or neck length is varied and also allows for more compact system. Special attention is paid to systems which exhibit multiple unstable modes and therefore need multiple Helmholtz resonators to be tuned in order to achieve stability. An algorithm for characterizing multiple unstable modes online is firstly developed, as described in section 2; this presents a particular challenge as FFT-based approaches do not promote fast-tracking of frequency shifts at low frequencies. A two-stage algorithm for tuning the HR neck areas online according to the characterization of the modes is developed in section 3. The performance of these algorithms is evaluated using a numerical model of an unstable combustion system with attached Helmholtz resonators in section 4. Finally, in section 5, we experimentally demonstrate that a simple combustion system with multiple unstable modes can be stabilized by tuning the neck areas of multiple Helmholtz resonators.

2 The online algorithm for characterizing modes

The frequencies of combustion instabilities tend to be close to the acoustic resonance frequencies of the combustion system, with the pressure oscillations occurring in the corresponding mode shape [17]. To effectively control combustion instabilities, the characteristics of the unstable modes (such as frequency and amplitude) need to be known. To identify these in real-time, as is needed for tuned passive control, an online mode-identification algorithm has been developed. It is performed in the time domain and allows faster tracking of changes due to changes in operating condition than would be possible using an FFT, particularly at low frequencies. Zinn and Neumeier [18,19] developed a similar algorithm and applied it with considerable success to active control of combustion instabilities. We now develop an algorithm for tuned passive control, which utilizes increases in computing speeds over the last decade.

2.1 Theory for the mode-identification algorithm

The mode-identification algorithm is based on the principle that integrating the product of a signal and a sinusoid over a period of the sinusoid extracts the component of the signal at the frequency of the sinusoid. Following the approach of Neumeier and Zinn [19], the measured pressure signal $P(t)$ is assumed to consist of N modes at frequencies Ω_n. It is then assumed that there is a dominant mode at frequency Ω_d. The pressure variation due to this dominant mode is denoted by $P_d(t)$. Since this mode dominates the measured pressure, it is initially assumed that $P(t) \approx P_d(t)$, which gives that $P(t)$ and its first derivative, $\dot{P(t)}$ can be expressed as,

$$P(t) = \sum_{n=1}^{N} (A_n \sin \Omega_n t + B_n \cos \Omega_n t) \approx A_d(t) \sin \Omega_d t + B_d(t) \cos \Omega_d t \tag{1}$$

$$\dot{P}(t) = \sum_{n=1}^{N} \Omega_n (A_n \cos \Omega_n t - B_n \sin \Omega_n t) \approx \Omega_d (A_d(t) \cos \Omega_d t - B_d(t) \sin \Omega_d t) \tag{2}$$

If the frequency of this mode, Ω_d, was known then the amplitude components of the dominant mode $A_d(t)$ and $B_d(t)$ could be determined by the short-time Fourier-like integrals shown in Eq. (3), where $T_d = 2\pi/\Omega_d$ and $\mathrm{j} = \sqrt{-1}$.

$$H(\mathrm{j}\Omega_d, t) = \frac{2}{T_d} \int_{t-T_d}^{t} P(\theta) \mathrm{e}^{-\mathrm{j}\Omega_d \theta} \, \mathrm{d}\theta = B_d(t) - \mathrm{j} A_d(t) \tag{3}$$

Because the dominant frequency is not known, an estimation of it, denoted by ω_d (with corresponding period τ_d) is used to perform the short-time Fourier-like integrations. The integration components, $s_d(t)$ and $c_d(t)$, are then taken to be approximations to $A_d(t)$ and $B_d(t)$.

$$G(\mathrm{j}\omega_d, t) = \frac{2}{\tau_d} \int_{t-\tau_d}^{t} P(\theta) \mathrm{e}^{-\mathrm{j}\omega_d \theta} \, \mathrm{d}\theta = c_d(t) - \mathrm{j} s_d(t) \tag{4a}$$

$$c_d(t) = \frac{\omega_d \Big[\Big(\dot{P}(t) - \dot{P}(t-\tau_d) \Big) \sin \omega_d t + \omega_d \Big(P(t) - P(t-\tau_d) \Big) \cos \omega_d t \Big]}{\pi(\omega_d^2 - \Omega_d^2)} \tag{4b}$$

$$s_d(t) = \frac{\omega_d \Big[\Big(\dot{P}(t) - \dot{P}(t-\tau_d) \Big) \sin \omega_d t - \omega_d \Big(P(t) - P(t-\tau_d) \Big) \cos \omega_d t \Big]}{\pi(\omega_d^2 - \Omega_d^2)} \tag{4c}$$

If ω_d converges to Ω_d, it can be seen from Eqs. (3) and (4a) that the amplitude components of $c_d(t)$ and $s_d(t)$ will converge to $B_d(t)$ and $A_d(t)$ respectively. Therefore, the signal defined as $p_d^s(t) = s_d(t) \sin \omega_d t + c_d(t) \cos \omega_d t$ is an approximation to the signal of the dominant mode, $P_d(t) = A_d(t) \sin \Omega_d t + B_d(t) \cos \Omega_d t$. Note that we perform the numerical integrations fully for $s_d(t)$ and $c_d(t)$ at each time step, unlike the approach used by Neumeier and Zinn

[19].

Eliminating $\dot{P}(t) - \dot{P}(t-\tau_d)$ from Eqs. (4b) and (4c) gives Ω_d in terms of ω_d,

$$\Omega_d^2 = \left(\omega_d^2 + \frac{\omega_d^2}{\pi} \frac{\Big[P(t) - P(t-\tau_d) \Big]}{[s_d(t)\cos\omega_d t - c_d(t)\sin\omega_d t]} \right) \tag{5}$$

Eq. (5) can be iteratively used to determine the frequency of the dominant mode of $P(t)$. A relaxation coefficient is used in practice to ensure smoother convergence. Eq. (4) then allows the amplitude and the phase of this mode to be iteratively deduced. Once the characteristics of the dominant mode have converged, the dominant mode is subtracted from the pressure signal $P(t)$. The remaining signal, $P(t) - P_d(t)$, is then used to characterise the next most dominant mode, following the same procedure as above. This modal identification and subtraction procedure can be repeated several times so that many modes are characterised.

2.2 Performance of the mode-identification algorithm

The mode identification algorithm was applied to a pressure signal measured on the experimental unstable combustion rig at the University of Cambridge [20]. Because the rig was undergoing limit cycle oscillations, the non-linearity limiting the amplitude meant that both the instability frequency and its first harmonic were strongly present. A sample rate of 5000 Hz was used and the algorithm was switched on at time 3.1 s. The results are shown in Fig. 1. Both modes are characterised with channel 1 representing the dominant mode and channel 2 the first harmonic. The frequencies and amplitudes of these two modes are time-dependent and shown in Fig. 1(a) and (b) respectively, with FFT results shown in Fig. 1(c) for comparison. The dominant mode is

characterised within 5 milliseconds and the first harmonic component within 50 milliseconds. The online algorithm is seen to reliably characterise both modes in terms of their frequencies and amplitudes.

A key feature of the algorithm is that it can rapidly track large changes in operating condition. This was demonstrated using a pressure signal measured in a cuboid-shaped tube with one end closed and one end open. The tube contained a loudspeaker, whose forcing frequency varied significantly with time. The mode-identification algorithm was applied to the pressure measurement. The actual forcing frequency and the predicted dominant frequency are shown in Fig. 2. The frequency predicted by the online algorithm closely tracks the changes in the forcing frequency with a very small time delay.

Thus it has been shown that the mode-identification algorithm can both identify the essential features of multiple modes, and track their changes in real time.

3 Two-stage tuning algorithm

In order to use the information obtained about the modes present to rapidly tune the neck areas of the Helmholtz resonators, a two-stage control algorithm was developed. The idea is that a separate HR is tuned for each separate mode, although this could be extended to tuning a set of HRs for each mode. The algorithm consists of an initial tuning stage and a fine-tuning stage, as shown schematically in Fig. 3. In the initial tuning stage, the modal frequency, as predicted by the mode-identification algorithm, is used to obtain a fast estimate of the optimum neck radius. The fine-tuning stage then involves

performing an online search to find the neck radius that minimises the modal amplitude. Fine-tuning is needed because the presence of a HR results in a shift in the mode frequency and hence the mode shape which is difficult to predict; amplitude minimisation is the most reliable way of obtaining the optimum neck radius.

The initial tuning stage is designed to give a quick response to variations in the frequency of the combustion instabilities as the operating conditions change. It uses the modal frequency provided by the mode-identification algorithm to estimate the optimum neck radius via the linear Helmholtz resonator equation $\omega^2 = c^2 S/V l_{\text{eff}}$. At each time step, the 'initial guess' is used only if the predicted frequency differs from the previously stored resonant frequency by more than a specified value.

The fine-tuning stage involves minimising the modal amplitude. The modal amplitude is provided by the mode identification algorithm and a revised Newton-Raphson algorithm is used to perform the minimisation, as shown in Eq. (6).

$$r_{n+1} = r_n - \alpha \frac{\frac{\partial \hat{p}_{(r_n)}}{\partial r}}{|\frac{\partial^2 \hat{p}_{(r_n)}}{\partial r^2}|} \tag{6}$$

Here, r is the neck radius of the resonator, α is a relaxation coefficient and $\hat{p}$ is the pressure modal amplitude. The relaxation coefficient avoids divergence. The full forms of $\frac{\partial \hat{p}}{\partial r}$ and $\frac{\partial^2 \hat{p}}{\partial r^2}$ can be found in [12]. Note in Eq. (6) the condition of $\frac{\partial^2 \hat{p}_{(r_n)}}{\partial r^2} > 0$ is necessary to guarantee finding a pressure amplitude minima other than maxima.

4 Numerical model with two unstable modes

The online mode-identification algorithm and two-stage tuning algorithm are now used to demonstrate tuned passive control in a numerical model. An axial combustion system with a choked upstream end and open downstream end is simulated as shown in Fig. 4. The combustor has two Helmholtz resonators, HR_1 and HR_2, attached; the neck areas of both can be varied.

The mean flow is assumed to be steady and one-dimensional, undergoing a change only across the flame. The flow fluctuations are modelled as being due to plane acoustic waves travelling in opposite directions. The wave strengths are denoted by $R_a(t)$, $L_a(t)$, $R_{b1}(t)$, $L_{b1}(t)$, $R_{b2}(t)$, $L_{b2}(t)$, $R_{b3}(t)$ and $L_{b3}(t)$ in the different combustion regions, as shown in Fig. 4. Entropy and vorticity contributions are neglected, and the acoustic waves are assumed to behave linearly with respect to the mean flow. The equations for the flow fluctuations upstream and downstream of the flame are given by

$$p'_a(x,t) = R_a\left(t - \frac{x}{\bar{c}_a + \bar{u}_a}\right) + L_a\left(t + \frac{x}{\bar{c}_a - \bar{u}_a}\right) \tag{7a}$$

$$u'_a(x,t) = \frac{1}{\bar{\rho}_a \bar{c}_a}\left[R_a\left(t - \frac{x}{\bar{c}_a + \bar{u}_a}\right) - L_a\left(t + \frac{x}{\bar{c}_a - \bar{u}_a}\right)\right] \tag{7b}$$

$$p'_{bi}(x,t) = R_{bi}\left(t - \frac{x}{\bar{c}_b + \bar{u}_b}\right) + L_{bi}\left(t + \frac{x}{\bar{c}_b - \bar{u}_b}\right) \tag{7c}$$

$$u'_{bi}(x,t) = \frac{1}{\bar{\rho}_b \bar{c}_b}\left[R_{bi}\left(t - \frac{x}{\bar{c}_b + \bar{u}_b}\right) - L_{bi}\left(t + \frac{x}{\bar{c}_b - \bar{u}_b}\right)\right] \tag{7d}$$

where p denotes the pressure, u is the flow velocity, ρ is the density, c the speed of sound and subscript i denotes the zone downstream of the flame. An over-bar denotes a mean value and a prime denotes a perturbation.

The combustor boundaries are modelled using pressure reflection coefficients. The Marble and Candel [21] expression is used for the choked upstream end

and the value -0.98 is used at the open downstream end. The flame is assumed to be sufficiently short compared to the acoustic wavelength that it can be modelled as a thin sheet. The acoustic wave strengths either side of the flame and the heat release fluctuation are related by applying the linearised flow conservation equations across the flame and assuming a form for the flame transfer function, $H(\omega) = Q(\omega)/u(\omega)$, where $Q(\omega)$ is the Fourier transform of the heat release fluctuation $Q'(t)$ and $u(\omega)$ is the Fourier transform of the velocity fluctuation $u'(t)$ just upstream of the flame. It is assumed that the heat release fluctuation can not exceed 20% of mean heat release i.e. a capping is imposed. This heat release saturation provides a non-linear mechanism by which a limit cycle occurs in the case of a combustion instability.

The acoustic wave strengths either side of each Helmholtz resonator are related by combining the flow conservation equations and a non-linear model of the HR damping. Mass and pressure continuity across each HR hold. The pressure loss across the neck of each HR is due to the non-linear effect of the 'jets' formed. This loss can be expressed in terms of a dynamic head loss, as shown in Eq. (8), where $\Delta p'$ is the pressure difference across the neck, $u'_h(t)$ is the acoustic flow velocity moving across the neck and K is the discharge coefficient taking account of the non-linear loss. This model has been used in several previous studies [5, 7, 12, 22].

$$\Delta p' = \bar{\rho}_i l_{\text{eff}} \frac{\partial u'_h(t)}{\partial t} + K \bar{\rho}_i u'_h(t) |u'_h(t)| \tag{8}$$

Thus the end boundary conditions and the flow conservation equations across the flame and the HRs provide enough information to solve for each of the eight wave strengths in Fig. 4. The resulting matrix equation is shown in Eq. (9), where A denotes the cross section area of the combustor, $\bar{M}$ the mean mach

number, S the neck area of Helmholtz resonator, u'_{HR} the velocity perturbation at the resonator neck and the $\mathbf{X}$ ands $\mathbf{Y}$ coefficient matrixes are shown in the Appendix.

$$\mathbf{X}\cdot\begin{pmatrix} L_a(t) \\ R_{b1}(t) \\ L_{b1}(t) \\ R_{b2}(t) \\ L_{b2}(t) \\ R_{b3}(t) \end{pmatrix} = \mathbf{Y}\cdot\begin{pmatrix} L_a\Big(t-\frac{2x_u}{\bar{c}_1(1-M_1^2)}\Big) \\ L_{b1}\Big(t-\frac{x_1}{(\bar{c}_2-\bar{u}_2)}\Big) \\ R_{b1}\Big(t-\frac{x_1}{(\bar{c}_2+\bar{u}_2)}\Big) \\ L_{b2}\Big(t-\frac{(x_2-x_1)}{(\bar{c}_2-\bar{u}_2)}\Big) \\ R_{b3}\Big(t-\frac{2(x_d-x_2)}{\bar{c}_2(1-M_2^2)}\Big) \\ R_{b2}\Big(t-\frac{(x_2-x_1)}{(\bar{c}_2+\bar{u}_2)}\Big) \end{pmatrix} + \begin{pmatrix} 0 \\ \frac{Q'}{A\bar{c}_1} \\ 0 \\ \frac{-\bar{\rho}_2\bar{c}_2S_1u'_{\mathrm{HR1}}(t)}{A} \\ 0 \\ \frac{-\bar{\rho}_2\bar{c}_2S_2u'_{\mathrm{HR2}}(t)}{A} \end{pmatrix} \tag{9}$$

The geometry of the combustor and the form of the flame transfer function [20] can be varied to give a combustion system which is either stable or unstable (with either one unstable mode or multiple unstable modes). For unstable systems, fluctuations grow exponentially in time until the heat release capping results in saturation into a limit cycle.

Before investigating the effectiveness of tuning the resonator neck areas for damping combustion instabilities, it is insightful to study how the variation of the resonator neck areas influences the acoustic response of the combustor. Fig. 5 demonstrates how the mode normalised amplitude, p'/p_0, and frequency, ω/ω_0, vary with the normalised radius of HR_1 $r_1/r_{1\max}$, with the neck area of HR_2 set to zero. Here, p_0 denotes the ambient pressure and ω_0 denotes the modal frequency in the absence of any HRs. The flame transfer function $H(\omega/\omega_0)$ is chosen to generate only one unstable mode at a normalised fre-

quency of 1.0. It is clear that the system is stabilised at some resonator neck areas. The shift in the modal frequency due to the presence of the HR is shown in Fig. 5(b), and depends on the resonator cavity volume and neck area. It is also apparent that a bad choice of neck area may result in a limit cycle with a larger amplitude.

In our work, the combustor lengths were chosen to be x_u=1.8 m and x_d=1.0 m, and the flame transfer function was chosen to be $H(\mathrm{j}\omega) = 3.21384 \times 10^8(\mathrm{j}\omega + 10)/\Big(-\omega^2 + 5000\mathrm{j}\omega + 2500^2\Big)$. It is worth noting that the form of $H(\mathrm{j}\omega)$ is specifically chosen to given two unstable modes. It is not intend to be a fully accurate representation of a real flame transfer function, although several of the features such as the high frequency roll-off beginning at 400 Hz are fairly realistic. The system exhibits two unstable modes, one at 239 Hz and one at 590 Hz. The frequency response plot of the transfer function from the unsteady heat release, $Q(\omega)$ to the measured pressure, $p_{\mathrm{ref}}(\omega)$ is shown in Fig. 6. An unstable mode is characterised by a phase increase of 180 degrees rather than a phase decrease [20]; the two unstable modes can clearly be seen.

The pressure 50 cm downstream of the flame provides the sensor signal for the online mode-identification algorithm. The predicted frequencies are used in the initial tuning of the two HR neck radii. HR_1 is set to damp the mode with a frequency of less than 500 Hz and HR_2 is set to the mode with a frequency higher than 500 Hz. The predicted amplitudes are used in fine-tuning to minimise the pressure amplitude.

The damping effect of the two HRs is presented in Fig. 7; this shows the effect of turning the HRs on one at a time, then deactivating them and turning them both on simultaneously. Both unstable modes at 239 Hz and 590 Hz are

initially present. The 239 Hz mode has the larger growth rate, and when the amplitude of this mode has grown large enough to cause saturation, nonlinear effects mean that the 590 Hz mode no long grows and the 239 Hz mode dominates completely in the first limit cycle. When tuning of HR_1 is activated at t=1 s, the dominant mode at 239 Hz is quickly eliminated. The 590 Hz mode is shifted slightly in frequency and begins to grow until saturation occurs and a larger amplitude limit cycle is established. Tuning the neck area of HR_2 begins at t=2 s; the recently established mode at 605 Hz disappears. At t=3 s, both HR_1 and HR_2 are turned off so that the original unstable mode at 239 Hz grows and re-dominates in the new limit cycle. At t=4 s, both HR_1 and HR_2 are turned on simultaneously. Both neck areas are simultaneously tuned and both the instabilities are sufficiently damped. It is noted that the optimum radius for the dominant mode is slightly different to that previously obtained; this is likely to be due to the different mode shape shifts that occur when both resonators are tuned simultaneously. It is apparent that with multiple unstable modes, multiple Helmholtz resonators are needed, especially when the modal frequencies are widely spaced.

This numerical simulation demonstrates that multiple unstable modes in combustion system can be attenuated by tuning neck areas of multiple Helmholtz resonators. This confirms that the online mode-identification algorithm and the two-stage tuning algorithm provide an effective and reliable combination for tuned passive control of combustion instabilities.

5 Experimental implementation

We now seek to apply our tuned passive control strategy experimentally in a self-excited combustion system. The Rijke tube [23, 24] is a simple and widely studied example of self-excited combustion system. It is typically a straight open-ended tube, with heat source, such as a flame inside. The requirements for instability are that there must be an air flow through the tube (e.g. due to natural convection), the heat source has to be in the upstream half of the tube, and the boundary losses must not be excessive.

In our work, in order to generate multiple modes, a novel Rijke tube which splits into two upper branches, shaped like a 'Y', was used, as shown in Fig. 8. The two upper branches had different lengths, and these provided a mechanism by which two instability frequencies (which were non-harmonic) could be obtained. The dimensions of the upper branches are $12 \times 6 \times 50$ cm and $12 \times 6 \times 90$ cm respectively, with the bottom 'stem' being $12 \times 8 \times 30$ cm. Attached to each upper branch was a Helmholtz resonator with an adjustable neck. The volumes and neck lengths of both HRs were 1.6×10^{-3} m^3 and 1.0×10^{-3} m respectively. The end correction used for the effective neck length, l_{eff} was 1.7 times of the neck radius.

The neck areas of the two Helmholtz resonators were both varied using 'iris' valves. The neck areas of both resonators can be approximately varied from 2.0×10^{-4} to 1.33×10^{-2} and from 1.0×10^{-4} to 5.0×10^{-3} m^2 respectively. Iris valves operate much like a camera lens, achieving a variable opening via rotating overlapping leaves. The 'iris' valves were driven by stepper motors, as shown in Fig. 8. Each stepper motor is controlled by three square waves

output from a computer. As the stepper motor rotates, the iris valves open or close. The iris valve blades are made from graphite coated stainless steel so that they can withstand relatively high temperatures. A methane-fueled Bunsen burner is used to provide a laminar flame, which heats a fine gauze of 10×5 cm. The flame and gauze both lie in the lower half of the tube, with the flame 7.0 cm from the lower tube end. With heating in place, the unstable modes are generated, with wavelengths corresponding to modeshapes within each branch. The pressure at 33 cm from the bottom 'stem' end was fed into the mode-identification algorithm. The online mode-identification algorithm and the two-stage neck area tuning algorithm were implemented in LabVIEW 8.0, with the data acquisition system consisting of a NI PCI-6229 card and two BNC 2090 connectors.

In Fig. 9, we show a sequence in which combustion instabilities establish themselves, occurring with a dominant modal peak at a frequency of 496 Hz and a secondary peak at a frequency of 328 Hz. The online mode-identification algorithm is switched on, followed by the passive tuning algorithm for both Helmholtz resonators at $t = 7.5$ s. HR_1 is attached to the short branch and set to damp the dominant mode, while HR_2 is attached to the long branch and is set to damp the secondary mode. The neck areas of HR_1 and HR_2 are quickly tuned, and the instabilities die away. Both Helmholtz resonators are deactivated at $t = 12$ s. By altering the fuel flow rate, two new modes at 355 Hz and 1020 Hz grow and the mode at 355 Hz becomes the new dominant mode. At time $t = 19.5$ s, the two resonators are switched on again. They retune their neck areas to the new modes so that these modes are quickly eliminated. The damping results in a sound pressure level reduction of more than 50 dB, as shown in Fig. 10.

The modeshapes within the two branches were measured during each of the two limit cycles, using the two microphone technique [25]. Six G.R.A.S. 1/4 inch Free field Microphones (Type 40BF) were used to measure pressure perturbations at different locations along both branches. They were attached to side arms along the branches, with the semi-infinite line technique used to obtain thermal insulation without distortion from acoustic reflections. The sound speed was obtained using local temperature measurements, and the mean flow speed was neglected. The mode shapes are shown in Fig. 11 (for the first limit cycle) and Fig. 12 (for the second). As expected, both mode shapes exhibit a pressure node near the open end. Note that the pressure mismatch between the two branches at the lower end is probably caused by the rapid area change at the join making the straight duct assumption invalid.

6 Discussion and conclusions

It has been shown that tuned passive control of combustion instabilities can be achieved by tuning the neck areas of Helmholtz resonators. The technique developed in this work placed emphasis on the ability to tune in real-time multiple Helmholtz resonators to damp multiple instability modes in the presence of varying operating conditions.

To identify the frequencies and amplitudes characterising the unstable modes present in a given combustion system, an online mode-identification algorithm was developed. This is a time-domain approach to identify and track modes online, faster than would be possible using an FFT. The frequencies and amplitudes for each separate mode are fed into a two-stage control algorithm for tuning the Helmholtz resonator neck areas (a separate resonator is currently

tuned for each mode). This algorithm consists of two stages, an initial tuning and a fine-tuning stage. The initial tuning stage gives a fast response to operating condition changes, while the fine-tuning performs an online minimisation of the modal amplitude.

The tuned passive control approach was firstly demonstrated on a numerical simulation of a longitudinal combustor with two unstable modes. It successfully damped both modes, confirming that the approach was numerically viable. It was then applied to a novel Rijke tube with two upper branches (a Y-shape), which exhibited multiple unstable modes. The Helmholtz resonator neck areas were varied by means of 'iris' valves, which operate like camera lenses. Again, the tuned passive control approach successfully eliminated both of the unstable modes.

In all, the tuned passive control approach developed by the authors was able to rapidly track the changes in the frequencies and modal amplitudes of combustion instabilities in real-time. It was thus able to damp these instabilities by varying Helmholtz resonator neck areas on the time scale of operating condition variations.

It is acknowledged that the temperature in real combustion systems, particularly in gas turbines, would make use of actuators such as the iris valve more of a technical challenge. Moreover, a mean flow through the resonators would be required for cooling purposes. This effect has not been included in the current work. Nonetheless, the mode identification algorithm and the principle of tuned passive control has been shown to be robust and effective, and it would now be interesting to adapt it for real industrial applications.

Acknowledgements

Dan Zhao's Ph.D studentship is funded by Cambridge Overseas Trust, Cambridge University Board of Graduate Studies and a Darwin College Scholarship. Dr Aimee Morgans was supported as a Research Fellow by the Royal Academy of Engineering and the EPSRC. This financial support is gratefully acknowledged. The authors thank Professor Dame Ann Dowling for her insights and suggestions and Mr John Hazelwood and Mr Dave Martin for their technical support in this work.

Appendix. Matrices X and Y

$$\mathbf{X} = \begin{pmatrix} -1+\bar{M}_1(2-\frac{\bar{u}_2}{\bar{u}_1})-\bar{M}_1^2 & 1+\bar{M}_1\frac{\bar{\rho}_1\bar{c}_1}{\bar{\rho}_2\bar{c}_2} & 0 & 0 & 0 & 0 \\ \frac{1-\gamma\bar{M}_1}{\gamma-1}+\bar{M}_1^2-\bar{M}_1^2(1-\bar{M}_1)\frac{1}{2}(\frac{\bar{u}_2^2}{\bar{u}_1^2}-1) & \frac{\bar{c}_2}{\bar{c}_1}\frac{1+\gamma\bar{M}_2}{\gamma-1}+\bar{M}_1\bar{M}_2\frac{\bar{\rho}_1}{\bar{\rho}_2} & 0 & 0 & 0 & 0 \\ 0 & 0 & 1 & -1 & 0 & 0 \\ 0 & 0 & 1 & 1 & 0 & 0 \\ 0 & 0 & 0 & 0 & 1 & -1 \\ 0 & 0 & 0 & 0 & 1 & 1 \end{pmatrix}$$

$$\mathbf{Y} = \begin{pmatrix} \frac{1-\bar{M}_1}{1+\bar{M}_1}\Big(1+\bar{M}_1(2-\frac{\bar{u}_2}{\bar{u}_1})+\bar{M}_1^2\Big) & -\Big(1-\bar{M}_1\frac{\bar{\rho}_1\bar{c}_1}{\bar{\rho}_2\bar{c}_2}\Big) & 0 & 0 & 0 & 0 \\ \frac{1-\bar{M}_1}{1+\bar{M}_1}\Big(\frac{1+\gamma\bar{M}_1}{\gamma-1}+\bar{M}_1^2 & & & & & \\ -\bar{M}_1^2(1+\bar{M}_1)\frac{1}{2}(\frac{\bar{u}_2^2}{\bar{u}_1^2}-1)\Big) & \frac{\bar{c}_2}{\bar{c}_1}\frac{1-\gamma\bar{M}_2}{\gamma-1}+\bar{M}_1\bar{M}_2\frac{\bar{\rho}_1}{\bar{\rho}_2} & 0 & 0 & 0 & 0 \\ 0 & 0 & -1 & 1 & 0 & 0 \\ 0 & 0 & 1 & 1 & 0 & 0 \\ 0 & 0 & 0 & 0 & 0.98 & -1 \\ 0 & 0 & 0 & 0 & 0.98 & 1 \end{pmatrix}$$

References

[1] T. C. Lieuwen, V. Yang, *Combustion instabilities in gas turbine engines*, American Institue of Aeronautics and Astronautics, Inc., 2005 8–25.

[2] A. S. Morgans, A. P. Dowling, Feedback control of combustion oscillations, *Annual Review of Fluid Mechanics* 37 (2005) 151–182.

[3] K. R. McManus, T. Poinsot, S. M. Candel, A review of active control of combustion instabilities, *Progress in Energy and Combustion Science* 19 (1993) 1–29.

[4] I. D. Dupere, A. P. Dowling, The use of Helmholtz resonators in a practical combustor, *Journal of Engineering for Gas Turbines and Power* 127 (2005) 268–275.

[5] B. T. Zinn, A theorectical study of non-linear damping by Helmholtz resonators, *Journal of Sound and Vibration* 13(3) (1970) 347–356.

[6] L. E. Kinsler, A. R. Frey, A. B. Coppens, J. V. Sanders, *Fundamentals of Acoustics*, John Wiley and Son Inc., 2000 272–291.

[7] A. Cummings, Acoustic nonlinearities and power losses at orifices, *AIAA Journal* 22 (1983) 786–792.

[8] A. P. Dowling, J. Ffowcs-Williams, *Sound and sources of sound*, Ellis Horwoood, 1983 130–135.

[9] J. M. DeBedout, M. A. Franchek, R. J. Bernhard, L. Mongeau, Adaptive-passive noise control with self-tuning Helmholtz resonators, *Journal of Sound and Vibration* 202(1) (1997) 109–123.

[10] K. Nagaya, Y. Hano, A. Suda, Silencer consisting of two-stage Helmholtz resonators with auto-tuning control, *Journal of Acoustical Society of America* (2001) 289–295.

[11] E. Little, A. R. Kashani, J. Kohler, F. Morrison, Tuning of an electrorheological fluid-based intelligent Helmholtz resonators as applied to hydraulic engine mounts, *ASME DSC Transportation Systems* (DE-76), (1994) 43–51.

[12] C.-H. Wang, Actively-tuned passive control of combustion instabilities, Ph.D. thesis, University of Cambridge, Engineering Department, Cambridge, UK 2004.

[13] S. Esteve, M. Johnson, Adaptive Helmholtz resonators and passive vibration absorbers for cylinder interior noise control, *Journal of Sound and Vibration* 288(4-5) (2005) 1105–1130.

[14] H. Matsuhisa, B. Ren, S. Sato, Semi-active control of duct noise by a volume-variable resonator, *JSME International Journal* 35(3) (1992) 223–228.

[15] S. Yamanaka, K. Shioda, Application of Helmholtz resonators for reducing the combustion oscillation in a gas turbine, *Proceedings of the International Gas Turbine Congress* (IGTC-TS-146), 2003.

[16] G. A. Richards, D. L. Straub, E. H. Robey, Passive control of combustion dynamics in stationary gas turbines, *Journal of Propulsion and Power* 19 (2003) 795–810.

[17] A. P. Dowling, S. R. Stow, Acoustic analysis of gas turbine combustors, *Journal of Propulsion and Power* 19(5) (2003) 751–764.

[18] Y. Neumeier, B. T. Zinn, Active control of combustion instabilities using real time identification of unstable combustion modes, *Proceedings of the 4th IEEE Conference on Control Applications* (1995) Albany, NY, USA.

[19] Y. Neumeier, N. Markopoulous, B. T. Zinn, A procedure for real time mode decomposition, observation, and prediction for active control of combustion instabilities, *Proceedings of the 1997 IEEE International Conference on Control Applications* Hartford, CT, USA, (1997) 818–823.

[20] A. S. Morgans, A. P. Dowling, Model-based control of combustion instabilities, *Journal of Sound and Vibration* 299 (2007) 261–282.

[21] F. E. Marble, S. M. Candel, Acoustic disturbance from gas non-uniformities convected through a nozzle, *Journal of Sound and Vibration* 55(2) (1977) 225–243.

[22] I. Day, A. P. Dowling, I. A. Dupere, C. Peyrache, Acoustic absorber for LPP combustors, Technical report, University of Cambridge, Engineering Department, 2001.

[23] P. L. Rijke, *Annalen der Physik* 107 (1859) 339–343.

[24] K. Matveev, Thermoacoustic instabilities in the Rijke tube: Experiments and modeling, Ph.D. thesis, California Institute of Technology, Pasadena, California, USA, February 7 2003.

[25] A. F. Seybert, D. F. Ross, Experimental determination of acoustic properties

using a two-microphone random-excitation technique, *Journal of the Acoustical Society of America* 61(5) (1977) 1362–1370.

Figure Captions

- Fig. 1(a) Modal frequencies predicted by the algorithm, (b) Modal amplitudes predicted by the algorithm, (c) FFT analysis of the pressure signal. The pressure signal was measured on the unstable combustion rig at the University of Cambridge: — Dominant mode, - - - Secondary mode.
- Fig. 2, Comparison between the loudspeaker forcing frequency and predicted frequency by the online mode-identification algorithm: - - - Forcing frequency, — predicted frequency by the algorithm.
- Fig. 3, Two-stage control scheme to tune HR neck radius.
- Fig. 4, A schematic of the combustor used in the numerical model.
- Fig. 5, The variations of the mode normalised amplitude and frequency with the resonator neck radius.
- Fig. 6, The open loop transfer function, $p_{ref}(\omega)/\ Q(\omega)$, analysis of a combustion system.
- Fig. 7, Numerical demonstration of the effect of tuned passive control on the numerical model: — Dominant mode in CH1, - - - Secondary mode in CH2.
- Fig. 8, The experimental apparatus in the Y-shape Rijke tube test: (a) the experimental Y shaped Rijke tube with two HRs attached, (b) the 'iris' valve used to vary the neck area.
- Fig. 9, The effect of tuned passive control on the Y-shape Rijke tube: $-\circ-$, HR1, $-\times-$, HR2.
- Fig. 10, Pressure spectra showing the typical damping effect of tuned passive control in the Y-shape Rijke tube test: —, 1st limit cycle, - - -, 2nd limit cycle, $\cdots$, after control.
- Fig. 11, Mode shape along each branch at the 1st limit cycle.

- Fig. 12, Mode shape along each branch at the 2nd limit cycle.

Figures

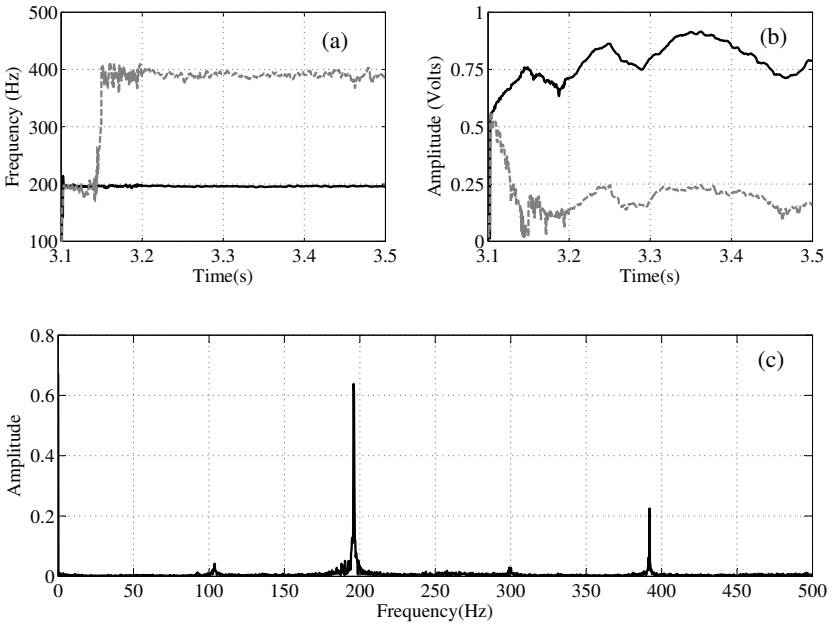

Fig. 1. (a) Modal frequencies predicted by the algorithm, (b) Modal amplitudes predicted by the algorithm, (c) FFT analysis of the pressure signal. The pressure signal was measured on the unstable combustion rig at the University of Cambridge: — Dominant mode, - - - Secondary mode.

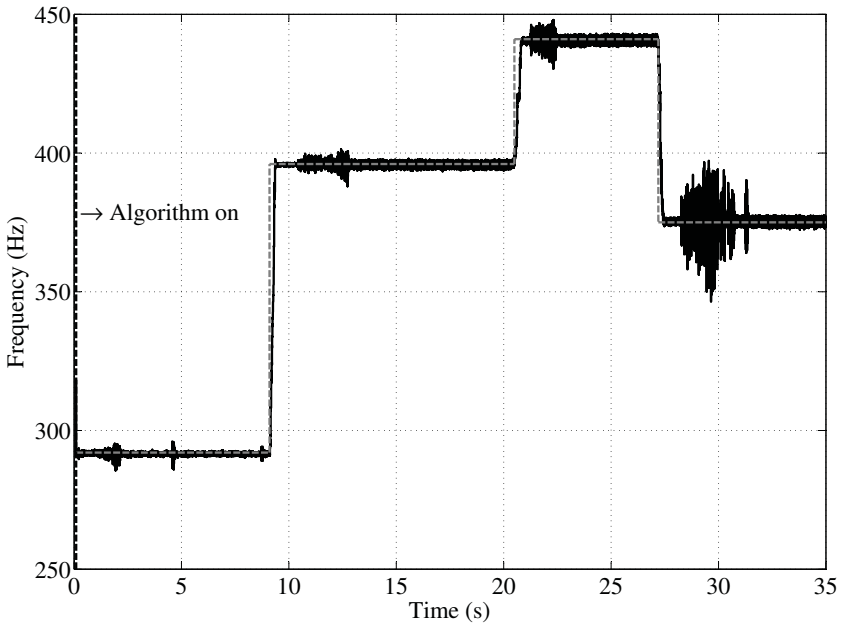

Fig. 2. Comparison between the loudspeaker forcing frequency and predicted frequency by the online mode-identification algorithm: - - - Forcing frequency, — predicted frequency by the algorithm.

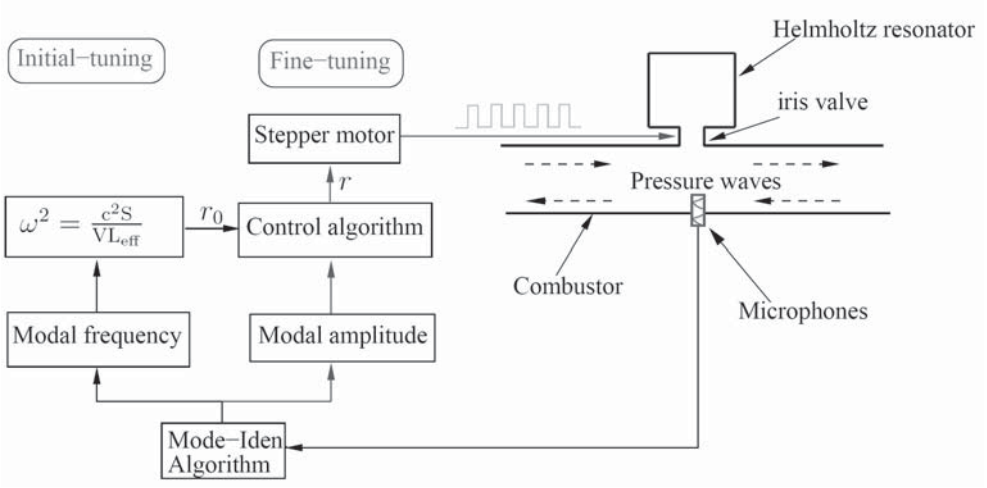

Fig. 3. Two-stage control scheme to tune HR neck radius.

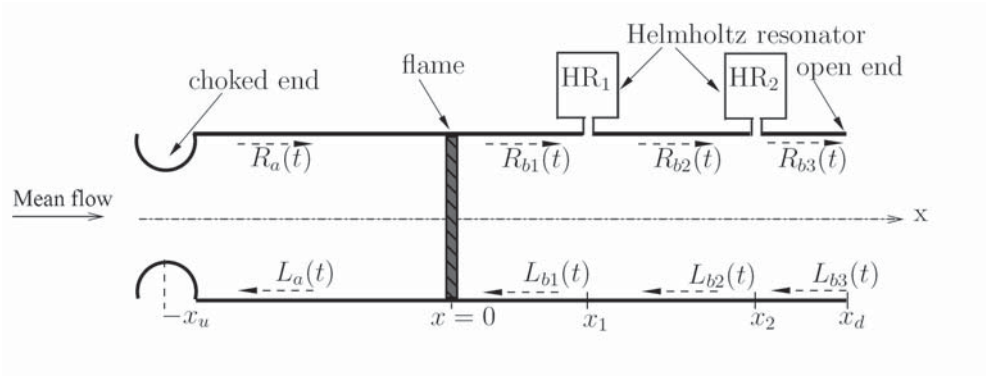

Fig. 4. A schematic of the combustor used in the numerical model.

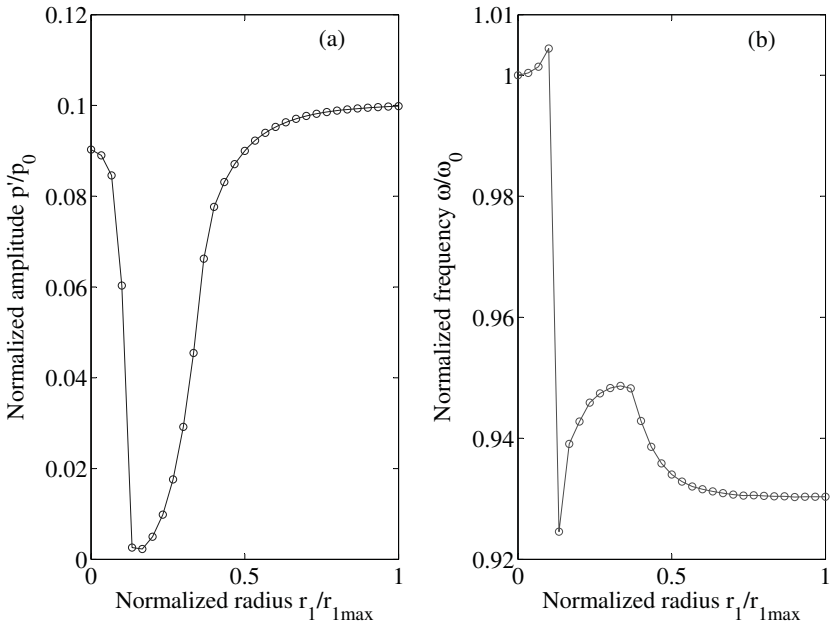

Fig. 5. The variations of the mode normalised amplitude and frequency with the resonator neck radius.

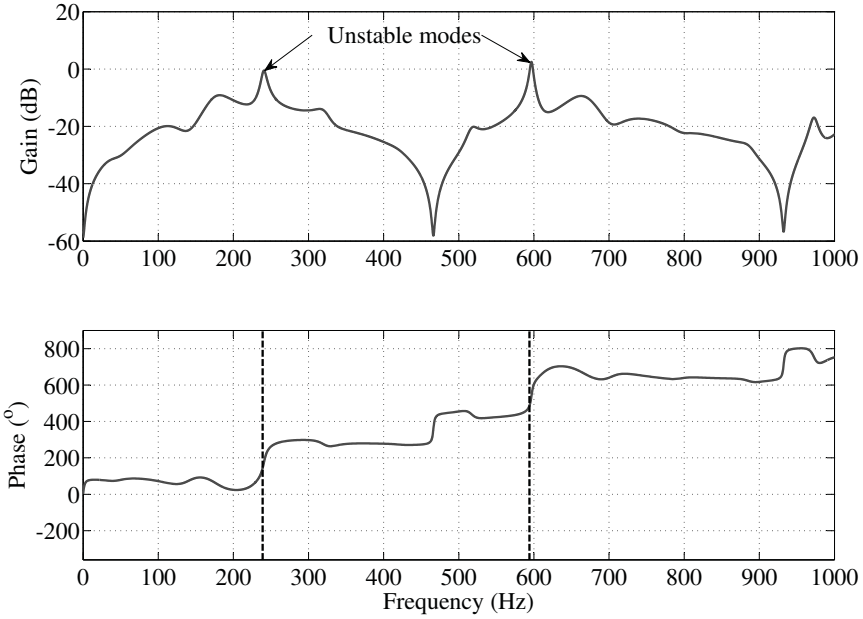

Fig. 6. The open loop transfer function, $p_{ref}(\omega)/\ Q(\omega)$, analysis of a combustion system.

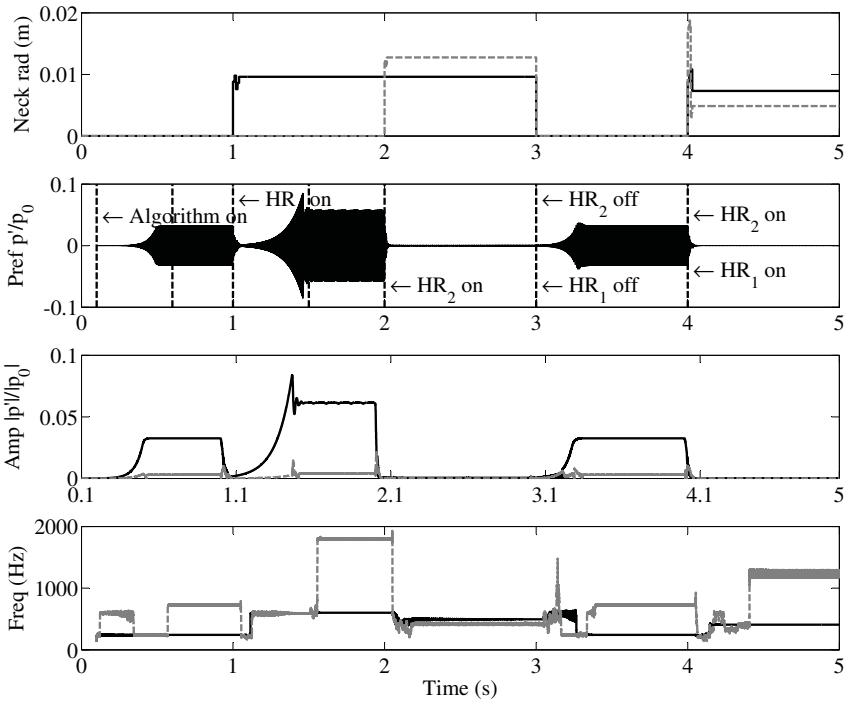

Fig. 7. Numerical demonstration of the effect of tuned passive control on the numerical model: — Dominant mode, - - - Secondary mode.

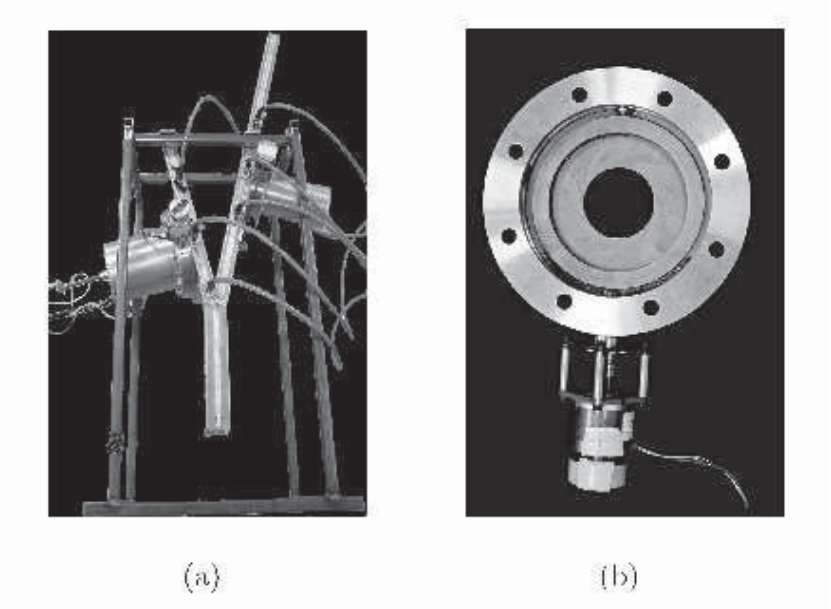

Fig. 8. The experimental apparatus in the Y-shape Rijke tube test: (a) the experimental Y shaped Rijke tube with two HRs attached, (b) the 'iris' valve used to vary the neck area.

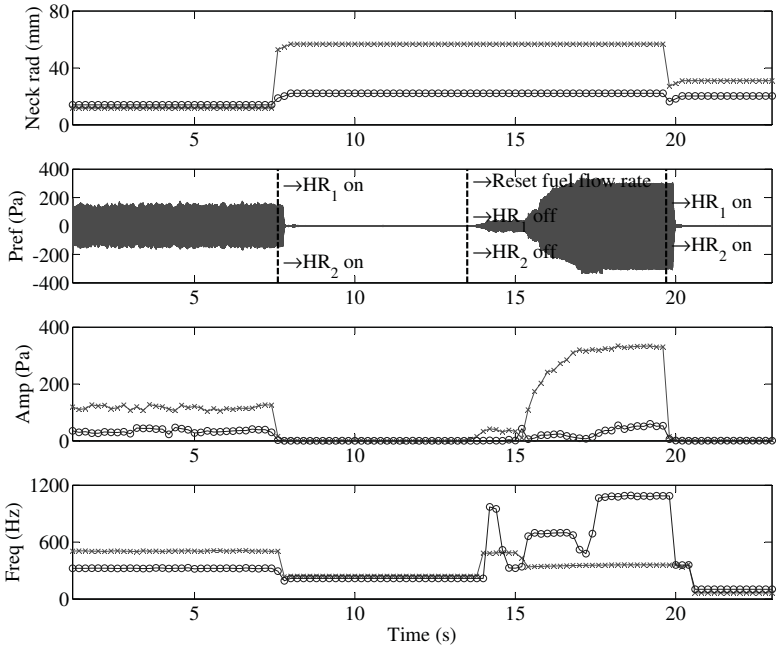

Fig. 9. The effect of tuned passive control on the Y-shape Rijke tube: $-\circ-$, HR1, $-\times-$, HR2.

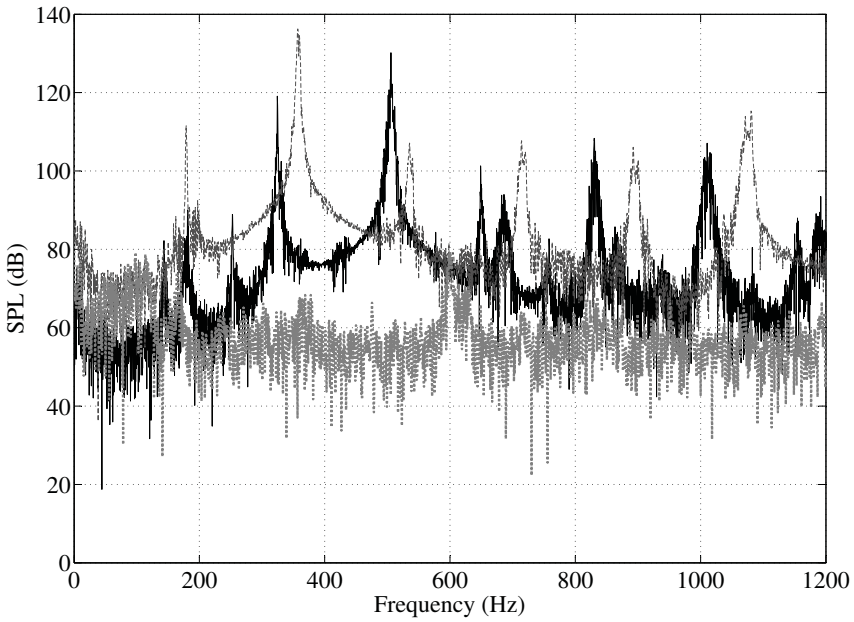

Fig. 10. Pressure spectra showing the typical damping effect of tuned passive control in the Y-shape Rijke tube test: —, 1st limit cycle, - - -, 2nd limit cycle, · · ·, after control.

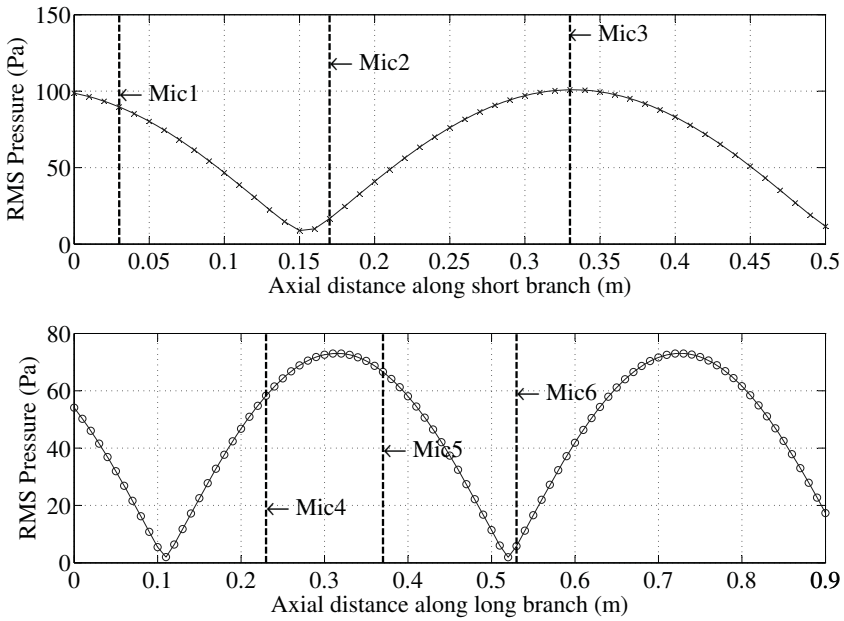

Fig. 11. Mode shape along each branch at the 1st limit cycle.

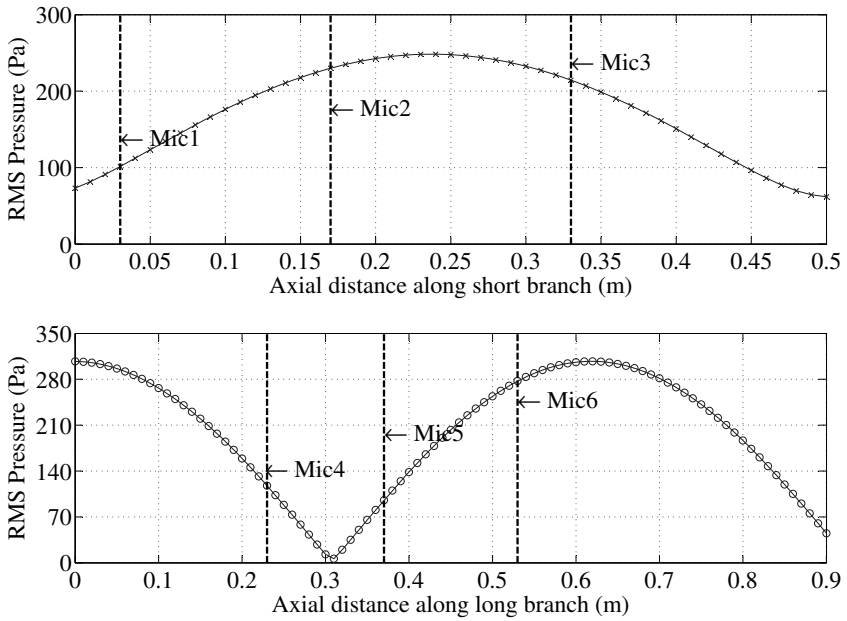

Fig. 12. Mode shape along each branch at the 2nd limit cycle.